Journal of Materials Chemistry B

ROYAL SOCIETY OF CHEMISTRY

PAPER

View Article Online
View Journal | View Issue

Cite this: J. Mater. Chem. B, 2020, 8, 1914

A distinctive mitochondrion-targeting, *in situ*-activatable near-infrared fluorescent probe for visualizing sulfur dioxide derivatives and their fluctuations *in vivo*†

Lintao Zeng, *[ab] Tianhong Chen,[ab] Bao-Quan Chen,[b] Hou-Qun Yuan,[c] Ruilong Sheng *[d] and Guang-Ming Bao *[c]

Received 18th November 2019,
Accepted 28th January 2020

DOI: 10.1039/c9tb02593f

rsc.li/materials-b

Sulfur dioxide derivatives are intimately involved in some physiological processes in organisms, and high levels of these substances can cause many diseases. Herein, we rationally prepared a mitochondrion-targeting, *in situ*-activatable near-infrared (NIR) fluorescent probe (**DCQN**) by coupling 2-(3,5,5-trimethylcyclohex-2-enylidene)malononitrile with 3-quinolinium carboxaldehyde. **DCQN** displayed a NIR fluorescence turn-on signal to indicate the presence of HSO_3^-, along with a considerable hyperchromic shift from light yellow to purple *via* a 1,4-nucleophilic addition reaction. We were able to use **DCQN** to instantaneously and quantitatively determine the concentration of HSO_3^- with high specificity, a low detection limit (24 nM), a large Stokes shift (~110 nm), and a high contrast ratio. Moreover, **DCQN** displayed good mitochondrion-targeting abilities and was *in situ*-activated by HSO_3^- to produce NIR fluorescence for imaging HSO_3^- in the mitochondria of live breast cancer cells. Furthermore, **DCQN** was used to monitor HSO_3^- in zebrafish with a high contrast ratio.

Introduction

Sulfur dioxide (SO_2) in the atmosphere generally originates from the combustion of fossil fuels such as coal and petroleum. SO_2 is colorless and can enter the body through the respiratory system and in this way pose a great threat to the health of organisms.[1–4] It becomes sulfite (SO_3^{2-}) and bisulfite (HSO_3^-) after being inhaled.[5] Exposure to high levels of SO_2 has been shown to lead to serious diseases such as acute respiratory syndrome, cardiovascular disease, lung cancer, and neurological disorders.[6–9] In particular, SO_2 and its derivatives can cause damage to mitochondria,[10–12] and such damage further triggers various sicknesses and dysfunctions[13] including cell malignancy, Alzheimer's disease, Parkinson's disease and atherosclerosis.[14] Thus, it is necessary to monitor the levels of SO_2 derivatives in live organisms.[15–19]

Fluorescent probes have attracted great attention due to their high sensitivity and selectivity, ability to detect targets non-invasively, and fluorescence imaging.[20–28] To date, several fluorescent probes have been developed for sensing bisulfite based on various reaction mechanisms, including nucleophilic reactions of aldehydes,[29,30] selective deprotection of levulinate,[31–33] Michael-type additions[34–36] and coordinative interactions.[37] These probes efficiently detect bisulfite in food and live cells, but few of them have been effectively used for *in situ* sensing and imaging *in vivo*. The main obstacles are that these probes, being typically small molecules, often tend to diffuse across the cell membrane without targeting the mitochondria while endogenous SO_2 derivatives are mainly generated within the mitochondria of live cells, some display short emission wavelength that cannot penetrate deep into tissues after reaction with bisulfite, and some are susceptible to nucleophilic reagents and enzymes (*e.g.*, esterases).[38–40] These drawbacks have inspired us to pursue the development of highly specific, rapid-response, mitochondrion-targeting *in situ*-activatable NIR fluorescent probes for imaging sulfur dioxide derivatives *in vivo*.[41]

Near-infrared (NIR) fluorescent probes offer a powerful tool to track and image some analytes *in vivo* by virtue of their low auto-fluorescence interference, their deep tissue-penetrability and the relatively little damage they inflict on biological samples.[42,43] In the current work, we designed and synthesized a mitochondrion-targeting and *in situ*-activatable NIR fluorescent

[a] College of Chemistry and Materials Science, Hubei Engineering University, Hubei, Xiaogan 432100, P. R. China. E-mail: zlt1981@126.com
[b] Tianjin Key Laboratory of Organic Solar Cells and Photochemical Conversion, Tianjin University of Technology, Tianjin, 300384, P. R. China
[c] School of Animal Science and Technology, Jiangxi Agricultural University, Nanchang 330045, P. R. China. E-mail: bycb2005@gmail.com
[d] CQM-Centro de Quimica da Madeira, Universidade da Madeira, Campus da Penteada, 9000-390, Funchal, Madeira, Portugal. E-mail: ruilong.sheng@staff.uma.pt; Fax: +351 291705254

† Electronic supplementary information (ESI) available: Experimental details and characterization data from the probe. See DOI: 10.1039/c9tb02593f

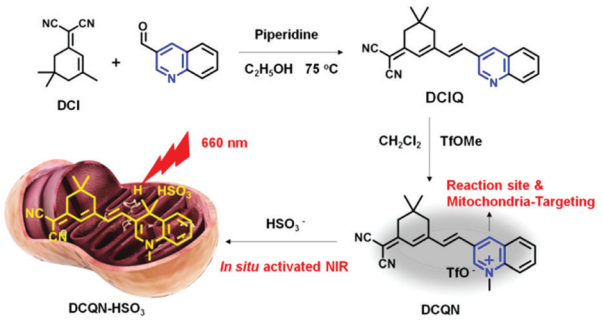

Scheme 1 Synthesis and working mechanism of the probe **DCQN**.

probe, **DCQN**, (Scheme 1) for imaging HSO_3^- *in vivo*. The quinolinium moiety of **DCQN** was shown to react with HSO_3^- *via* a 1,4-nucleophilic addition reaction to form product with a donor-π-conjugation-acceptor (D–π–A) structure, a feature that gave rise to an obvious chromogenic reaction and activated strong NIR fluorescence. Due to the high specificity and efficiency of this 1,4-nucleophilic addition, **DCQN** exhibited high selectivity and sensitivity, a low detection limit, and a rapid response to HSO_3^-. Furthermore, **DCQN** was effectively employed as a fluorescence imaging agent for monitoring HSO_3^- and its fluctuations in live breast cancer (MCF-7) cells and zebrafish.

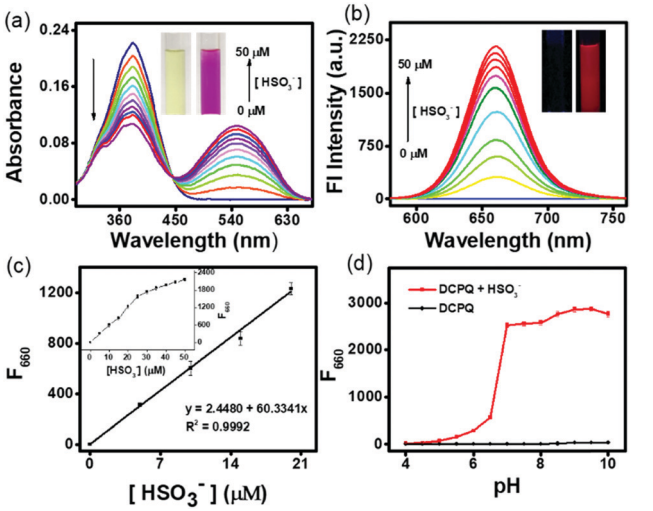

Fig. 1 (a) UV-vis absorption and (b) fluorescence spectra of **DCQN** (10 μM) in DMSO/HEPES buffer solution (v/v = 1/9, 10 mM, pH 7.4) with various amounts of added HSO_3^- (0–50.0 μM); inset: photographs of the **DCQN** solution before and after the addition of HSO_3^-. (c) The linear relationship between the fluorescence intensity of **DCQN** (10 μM) and the concentration of HSO_3^-. (d) Fluorescence response of **DCQN** (10 μM) to HSO_3^- (0.1 mM) in DMSO/HEPES solution (v/v = 1/9, 10 mM) at 25 °C as a function of pH. Each spectrum was recorded after incubation with HSO_3^- for 30 s. The excitation wavelength was 550 nm. Slits: 5/5 nm. The error bars represent ± SD, n = 3.

Results and discussion

Design and synthesis of DCQN

In this work, we rationally designed a structurally simple, low-cost, near-infrared-light-emitting and highly water-soluble probe, namely **DCQN**, by coupling 2-(3,5,5-trimethylcyclohex-2-enylidene) malononitrile (**DCI**) with 3-quinolinecarboxaldehyde, followed by performing a methyl trifluoromethanesulfonate (TfOMe)-mediated methylation. **DCQN** was designed to contain two electron-withdrawing groups, namely 1-methylquiolinium and malononitrile groups, to form an acceptor–π–conjugation-acceptor (A–π–A) structure that could quench the fluorescence of the probe.[44,45] And the 4-position of methylquinolinium offered a potential reduction site for HSO_3^-. We set out to react **DCQN** with HSO_3^- in order to form an electron-rich enamine moiety, and hence resulting in a favorable D–π–A structure and a typical intermolecular charge transfer (ICT) effect. Consequently, we observed an evident hyperchromic effect and NIR fluorescence "turn-on" emission with a large Stokes shift. **DCQN** was readily synthesized using conventional synthesis routes, as depicted in Scheme 1. The chemical structures of **DCQN** and its intermediates were confirmed using ^{1}H NMR, ^{13}C NMR and HRMS, as shown in ESI† (Fig. S8–S13).

Spectral responses of DCQN towards HSO_3^-

The optical sensing of **DCQN** towards HSO_3^- was investigated using a DMSO/HEPES buffer solution (v/v = 1/9, 10 mM, pH 7.4) at 25 °C. As shown in Fig. 1(a), **DCQN** displayed a strong absorption peak at a wavelength of 380 nm. Upon addition of HSO_3^- (0–5 equiv.), the intrinsic absorption peak of **DCQN** at this wavelength gradually decreased, and a new peak at 550 nm emerged, affording an obvious hyperchromic shift from light yellow to purple. At the same time, a near-infrared fluorescence band at 660 nm (Φ_f = 0.12) was immediately observed with a large Stokes shift (Fig. 1b and Fig. S1, ESI†). This NIR fluorescent probe showed some merits such as high contrast ratio, relatively deep light penetration and low interference from background, and hence appeared to fully meet the requirements of imaging sulfur dioxide derivatives *in vivo*. Besides, a very highly linear correlation between fluorescence intensity (F_{660}, R^2 = 0.9992) and HSO_3^- concentration (0–20 μM) was observed (Fig. 1c), and the detection limit was 24 nM (Fig. S2, ESI†), suggesting that **DCQN** can be used to quantitatively detect HSO_3^- with high sensitivity. Since pH usually influences the sensing performances and chemical stabilities of probes, we investigated the fluorescence response of **DCQN** (10 μM) to 100 μM HSO_3^- in various pH conditions. As shown in Fig. 1(d), the fluorescence intensity (F_{660}) of **DCQN** remained nearly constant within the pH range of 4–10. Whereas the addition of bisulfite (100 μM) triggered a sharp fluorescence enhancement at pH 6–10. These observations demonstrated that the good pH stability and applicability of the **DCQN** probe under pH 7.4, which endowed it with great potential for use in biological applications.

We also carried out a time-course investigation of the fluorescence response of **DCQN** (10 μM) to HSO_3^- (100 μM). As shown in Fig. 2, F_{660} of **DCQN** (10 μM) initially dramatically increased and then reached a plateau at about 6 s after the addition of HSO_3^- (10 equiv.), suggesting the ability of **DCQN** to serve as an ultra-rapidly responding fluorescent probe for imaging HSO_3^-.

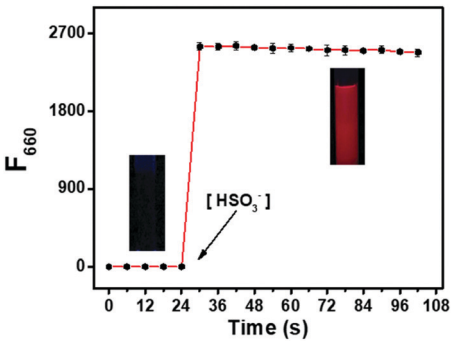

Fig. 2 Time course of the fluorescence response (F_{660}) of DCQN (10 μM) to HSO_3^- (100.0 μM) in HEPES buffer solution (10 mM, pH 7.4, with 10% DMSO, v/v) at 25 °C. The excitation wavelength was 550 nm. Slits: 5/5 nm, the error bars represent ± SD, n = 3.

Analyte selectivity

Considering the complexity of the intracellular environment, a fluorescent probe with high selectivity is desired for accurate and real-time imaging of bisulfite in biological systems. To evaluate the selectivity of **DCQN** (10 μM) for HSO_3^- (100 μM), a variety of biological species (100 μM) were examined, including common anions (Cl^-, Br^-, I^-, HCO_3^-, CO_3^{2-}, AcO^-, HPO_4^{2-}, SO_4^{2-}, $S_2O_3^{2-}$, $S_2O_7^{2-}$, SO_3^{2-} HS^-, and CN^-), nitroxides (NO_2^- and NO_3^-), amines ($NH_3{\cdot}H_2O$, $N_2H_4{\cdot}H_2O$, and n-$C_3H_7NH_2$), reactive oxygen species (ClO^- and H_2O_2) and bio-thiols (Cys, Hcy, and GSH). As shown in Fig. 3a, **DCQN** exhibited a negligible change in fluorescence and color upon the addition of any of test species except HSO_3^- and SO_3^{2-}. The addition of HSO_3^- or SO_3^{2-} caused an obvious hyperchromic shift from light yellow to purple together with a very strong enhancement of the fluorescence at 660 nm. Furthermore, we checked the selectivity of **DCQN** for HSO_3^- in the co-presence of other analytes. As shown in Fig. 3b, DCQN (10 μM) exhibited a remarkable fluorescence turn-on response to HSO_3^- (100 μM) even when any of various other anions and biological species (100 μM) was present. This finding indicated a high selectivity of the **DCQN** probe for HSO_3^- and that this probe might be effectively used in real biological systems.

Mechanism of the DCQN sensing of HSO_3^-

To gain some information about the mechanism of the reaction between **DCQN** and HSO_3^-, we conducted ^{1}H NMR titration experiments and HRMS analysis. As shown in Fig. 4, the proton chemical shifts of Ha and Hb in the quinolinium moiety appeared at 9.62 ppm and 9.27 ppm, respectively, and shifted to 6.42 ppm and 4.93 ppm after reaction with 18 equiv. of HSO_3^-. Meanwhile, the proton signal of Hc at 4.57 ppm assigned to the 1-position of the quinolinium moiety also shifted up-field (3.32 ppm). Analysis of the acquired ^{1}H NMR spectra revealed that the quinolinium group of **DCQN** was attacked by HSO_3^-, followed by a C=C bond rearrangement to form DCQN–HSO_3 with a D–π–A structure. The obtained HRMS results also confirmed the formation of the DCQN–HSO_3 adduct, as it showed a dominant peak at an m/z value of 420.1389 (calcd: 420.1387),

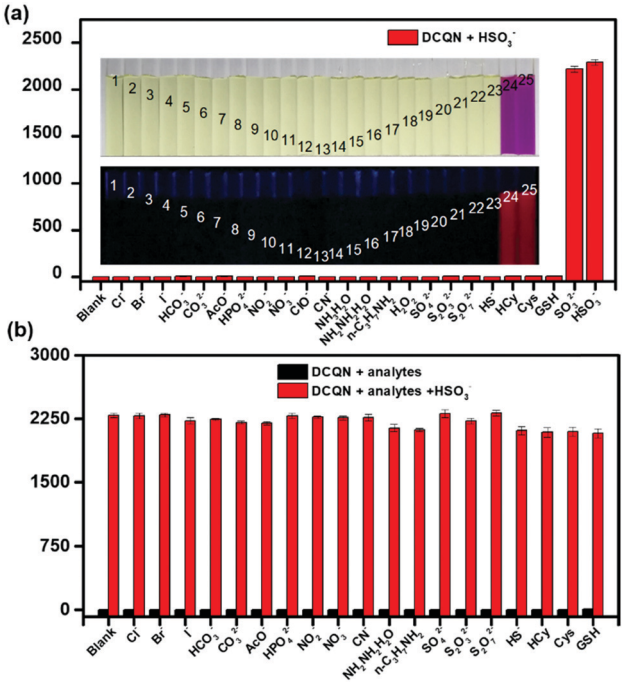

Fig. 3 Fluorescence responses of **DCQN** (10 μM) to various analytes (100.0 μM) in DMSO/HEPES buffer solution (v/v = 1/9, 10 mM, pH 7.4) at 25 °C. Each spectrum was recorded after 2 min. The excitation wavelength was 550 nm. Slits: 5/5 nm. Inset: Regular (upper) and fluorescence (bottom) photographs of **DCQN** (10 μM) in the presence of various species, specifically, from left to right: (1) blank, (2) Cl^-, (3) Br^- (4) I^-, (5) HCO_3^-, (6) CO_3^{2-}, (7) AcO^-, (8) HPO_4^{2-}, (9) NO_2^-, (10) NO_3^-, (11) ClO^-, (12) CN^-, (13) $NH_3{\cdot}H_2O$, (14) $N_2H_4{\cdot}H_2O$, (15) n-$C_3H_7NH_2$, (16) H_2O_2, (17) SO_4^{2-}, (18) $S_2O_3^{2-}$, (19) $S_2O_7^{2-}$, (20) HS^-, (21) Cys, (22) Hcy, (23) GSH, (24) SO_3^{2-}, and (25) HSO_3^-. Error bars represent ± SD, n = 3.

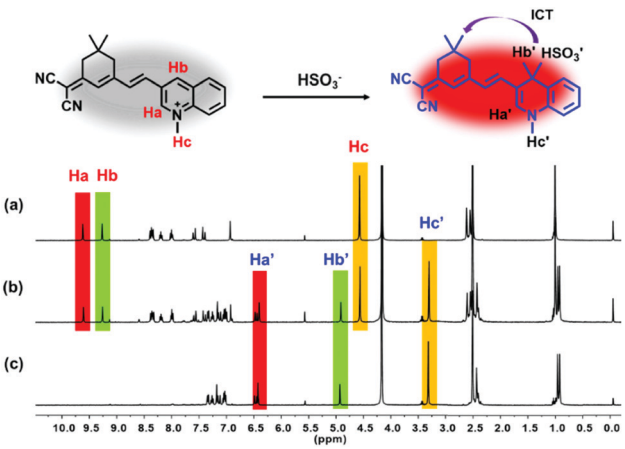

Fig. 4 ^{1}H NMR spectra of **DCQN** with (a) 0 equiv., (b) 9 equiv., and (c) 18 equiv. of HSO_3^-.

which corresponded to $[DCQN–HSO_3–H]^-$ (Fig. S3, ESI†). These results were in good agreement with the spectral behavior of **DCQN**, and verified that **DCQN** exhibited a dramatic hyperchromic shift and near-infrared fluorescence light-up in response to HSO_3^- due to a 1,4-Michael reaction between the quinolinium skeleton and HSO_3^-.

Cytotoxicity and fluorescence imaging for MCF-7 cells

Before **DCQN** was used to image HSO_3^- in MCF-7 cells, the cytotoxicity of **DCQN** was evaluated by performing a CCK-8 assay. As shown in Fig. 5, the cell survival rate remained above 87% after incubation with various concentrations of **DCQN** (0–25 μM) for 24 h, implying a good biocompatibility of **DCQN**. Encouraged by these favorable properties, we then utilized **DCQN** to image HSO_3^- in live MCF-7 cells. First, the MCF-7 cells were incubated with **DCQN** (10 μM) at 37 °C for 30 min and then fluorescence images of them were captured using laser confocal scanning microscopy. As shown in Fig. 6 and Fig. S4 (ESI†), MCF-7 cells were observed to be non-fluorescent in the red channel after incubation with **DCQN** for 30 min. Subsequently, these cells were incubated with HSO_3^- (0, 30 and 60 μM) for 10 min, and the images were recorded. Notably, these cells displayed clear red fluorescence cell profiles, and the fluorescence became much brighter as the concentration of HSO_3^- was increased. Notably, some albeit weak red fluorescence was observed in the cells incubated with **DCQN** and then HSO_3^- at a concentration as low as 250 nM (Fig. S5, ESI†), suggesting that **DCQN** could serve as a sensitive probe for efficiently imaging exogenous HSO_3^- in live cells. **DCQN** also displayed good optical stability in the live cells (shown in Fig. S6, ESI†). Thus, this NIR-light-emitting fluorescent probe was found to display several advantages such as good photostability, high contrast ratio and low background interference, which are favorable for imaging HSO_3^- *in vivo*.

Fluorescence imaging of HSO_3^- located in mitochondria

SO_2 derivatives also can be endogenously generated within mitochondria. To explore the mitochondria targeting and sensing ability of **DCQN** for HSO_3^-, MCF-7 cells were co- incubated with **DCQN** (10 μM) and the commercially available Mito-Tracker Green (200 nM) at 37 °C for 30 min. Afterwards, they were further incubated with HSO_3^- (60 μM) for another 10 min and their fluorescence images were recorded by using a confocal laser-scanning microscope. As shown in Fig. 7, we observed very clear red fluorescence profiles of mitochondria in the MCF-7 cells pre-incubated first with **DCQN** and then HSO_3^- (60 μM). The fluorescence co-localization of Mito-Tracker Green and **DCQN** overlapped essentially perfectly, and the corresponding Pearson's correlation coefficient was 0.95. Hence, **DCQN** was found to display an excellent mitochondrion-targeting ability and could be activated by exogenous bisulfite to generate NIR fluorescence inside mitochondria of live cells.

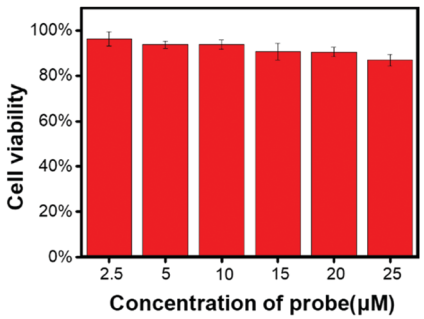

Fig. 5 MCF-7 cell viabilities after incubation with various concentrations of **DCQN** (0–25 μM) for 24 h. Error bars represent ± SD, n = 5.

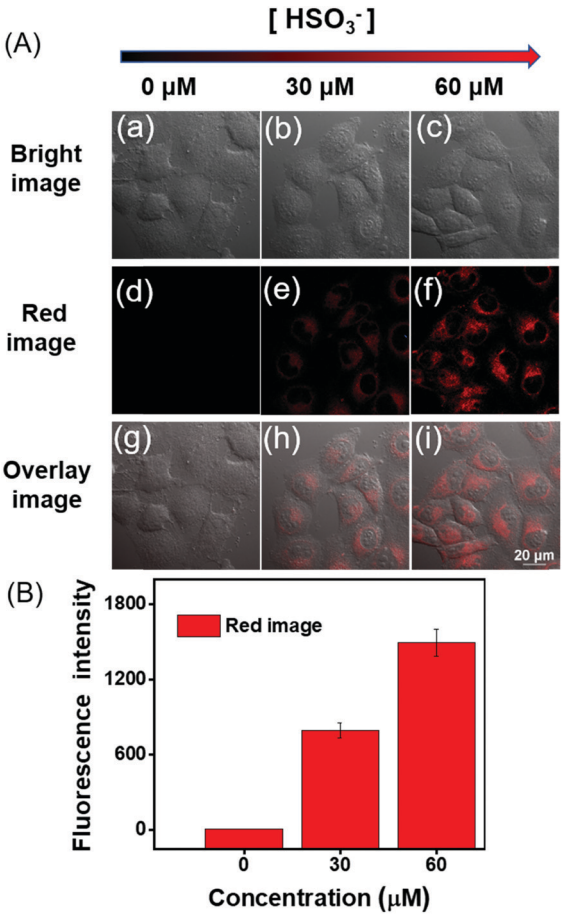

Fig. 6 (A) Confocal images of various samples of MCF-7 cells incubated with **DCQN** (10 μM) at 37 °C for 30 min, and then treated with different concentrations of HSO_3^- (0–60 μM) for 10 min. Cell images were acquired with $\lambda_{ex}/\lambda_{em}$ of 543/648–703 nm. Scale bar: 20 μm. (B) Statistical analysis based on the peak fluorescence intensity of MCF-7 cells. Error bars represent ± SD, n = 5.

Fluorescence imaging of HSO_3^- in zebrafish

In view of the above-described meritorious characteristics of **DCQN**, we further exploited the capability of **DCQN** for the fluorescence imaging of HSO_3^- *in vivo*. Zebrafish was used as the vertebrate organism to perform fluorescence imaging of HSO_3^- *in vivo*. As shown in Fig. 8, the zebrafish did not fluoresce when they were incubated with just **DCQN** (10 μM) for 30 min. These zebrafish were further incubated with different concentrations of HSO_3^- (0, 30, 60, 90 and 120 μM) for 10 min at 28 °C and images of them were acquired with a confocal laser-scanning microscopy. As expected, red fluorescence appeared within the zebrafish when HSO_3^- was included, and the fluorescence intensity became much stronger (red channel with $\lambda_{ex}/\lambda_{em}$ of 543/648–703 nm) as the HSO_3^- concentration was increased from 0 to 120 μM. The red fluorescence was mainly located at the contours of the eyes and abdomen (Fig. 8, enlarged red images), and became much

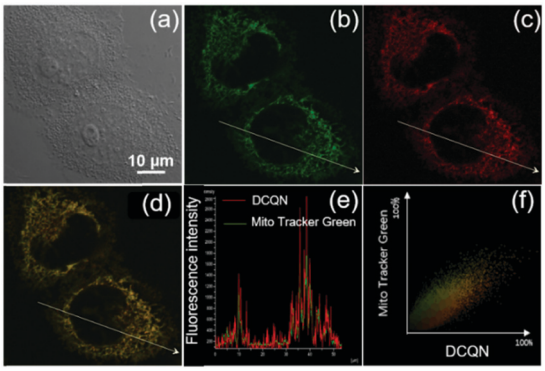

Fig. 7 Confocal images of MCF-7 cells stained with (b) 200 μM Mito Tracker Green (green channel $\lambda_{ex}/\lambda_{em}$ of 488/500–530 nm) and (c) 10 μM **DCQN** (red channel $\lambda_{ex}/\lambda_{em}$ of 543/648–703 nm) for 30 min and then further incubated with HSO_3^- (60 μM) for another 10 min in MCF-7 cells. (a) Bright images, (d) merged images, (e) intensity profile within the regions of interest, and (f) a correlation plot of Mito-Tracker Green and **DCQN** intensities. Pearson's correlation coefficient: 0.95. Scale bar: 10 μm.

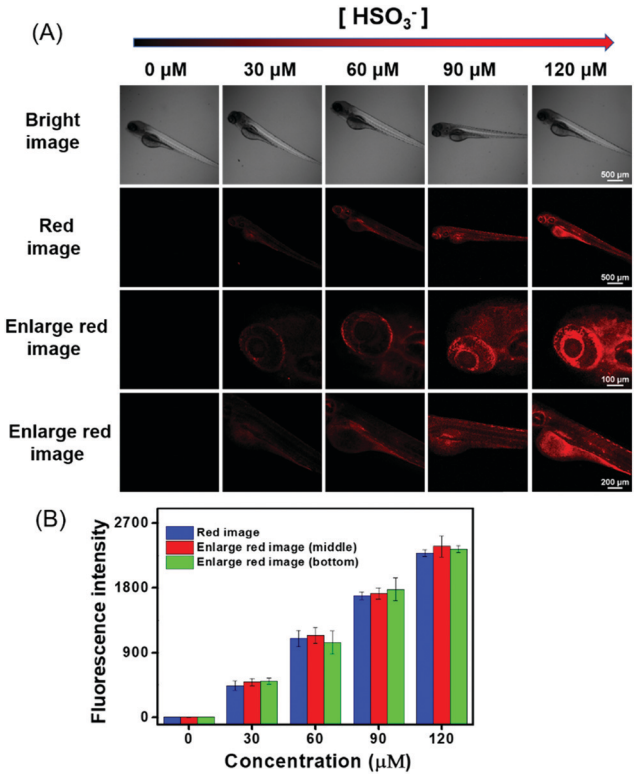

Fig. 8 (A) Confocal images of various four-day-old zebrafish pre-incubated with **DCQN** (10 μM) at 28 °C for 30 min, and then treated with different concentrations of HSO_3^- (0, 30, 60, 90, 120 μM) for 10 min. These images were acquired with λ_{ex} of 543 nm and emission wavelength between 648 and 703 nm. Scale bar: 500 μm. The local merged scale bar: 200 μm and 100 μm. (B) Statistical analysis based on peak fluorescence intensity of the zebrafish. Error bars represent ± SD, n = 5.

brighter here with the increase in HSO_3^- concentration. Hence, **DCQN** could be used to track bisulfite in living system. To further demonstrate the excellent imaging ability of **DCQN**, the zebrafish were first incubated with **DCQN** (10 μM) for 30 min,

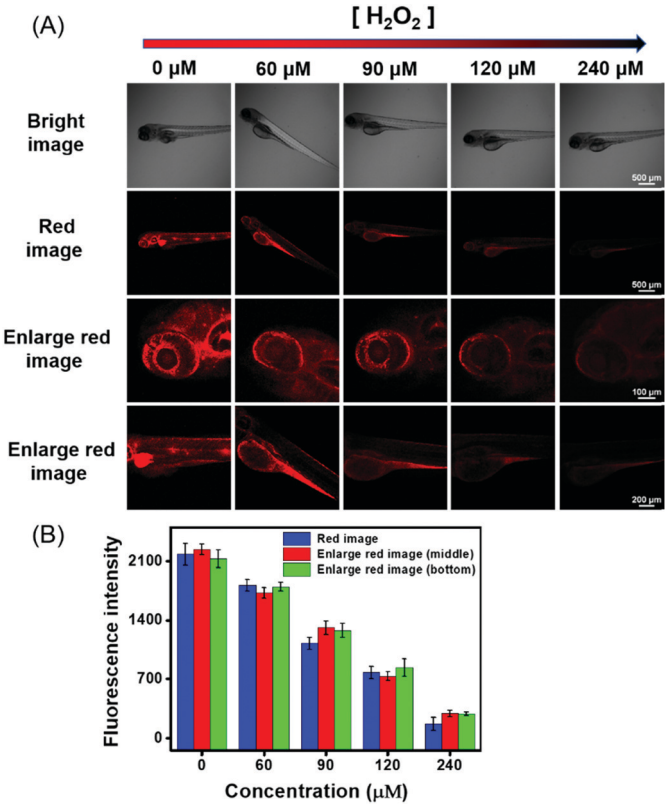

Fig. 9 (A) Confocal images of four-day-old zebrafish loaded with **DCQN** (10 μM) at 28 °C for 30 min, followed by being incubated with HSO_3^- (120 μM) for 10 min, and then with different concentrations of H_2O_2 (0, 60, 90, 120, and 240 μM) for 10 min at 28 °C. These images were acquired with λ_{ex} of 543 nm and emission wavelengths between 648 and 703 nm. Scale bar: 500 μm. The local merged scale bars were 200 μm and 100 μm, respectively. (B) Statistical analysis based on the peak fluorescence intensity of the zebrafish. Error bars represent ± SD, n = 5.

then stimulated with HSO_3^- (120 μM) for 10 min, and finally treated with different concentrations of H_2O_2 (0, 60, 90, 120 and 240 μM) for another 10 min, after which fluorescence images of these zebrafish were recorded. As shown in Fig. 9, while very strong red fluorescence was observed within the zebrafish incubated with just **DCQN** and HSO_3^-, the intensity of the fluorescence decreased as the H_2O_2 concentration was increased from (0 to 240 μM), which again confirmed the good imaging ability of **DCQN**. Moreover, these observations implied that the SO_2 derivative and DCQN–HSO_3 could be oxidized by H_2O_2. Hence, according to our results, **DCQN** can be employed as an *in vivo* NIR imaging agent to visually study the process of the detoxification of sulfur dioxide derivatives with oxidants. Further research about this function is expected to be carried out in the near future.

In vivo fluorescence imaging of HSO_3^- during the growth and development of zebrafish

Sulfur dioxide derivatives have been previously shown to cause oxidative damage to living organisms.[46,47] Herein, we further explored the absorption of HSO_3^- and its distribution in the body during the growth and development of zebrafish.

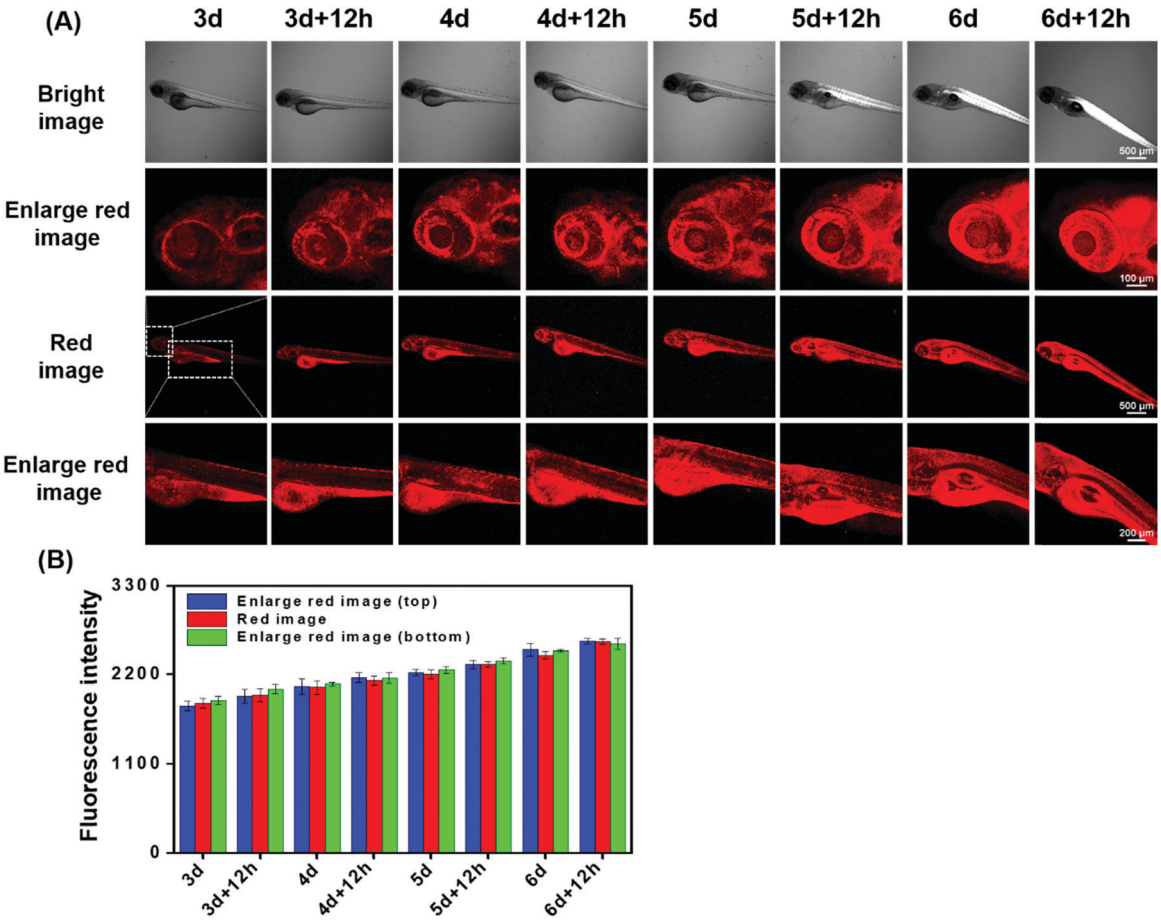

Fig. 10 (A) Confocal images of different zebrafish incubated with **DCQN** (10 μM) at 28 °C for 30 min, and then treated with HSO_3^- (120 μM) for 10 min. These images were acquired with λ_{ex} of 543 nm and emission wavelengths between 648 and 703 nm. Scale bar: 500 μm. The partial imaging scale bar: 200 μm and 100 μm. (B) Statistical analysis based on the peak fluorescent intensity of the zebrafish. Error bars represent ± SD, n = 5.

Zebrafish between three and six days of age were pre-incubated with **DCQN** (10 μM) for 30 min at 28 °C, and further treated with HSO_3^- (120 μM) for 10 min. As shown in Fig. 10, bright red fluorescence in the entire body of zebrafish was boosted by HSO_3^-. This result implied that HSO_3^- can quickly enter and spread throughout the whole body, and hence subsequently possibly cause systemic oxidation-associated injury. Interestingly, red fluorescence (shown in Fig. 10, enlarged red image) was much brighter at the head, intestines and abdomen than at other body parts. This result indicated that sulfur dioxide derivatives would tend to accumulate in these organs and may subsequently damage them, thereby causing local pathological changes. Also, the fluorescence intensity in the zebrafish became much stronger as the culture time was prolonged. To our delight, we clearly observed the development of the eyeballs, abdomen and head. Apparently, various organs of the zebrafish gradually matured and showed their morphologies in the presence of HSO_3^- (120 μM) (Fig. S7, ESI†). The fluorescence enhancement with increased growth time may be attributed to the enhancement of the digestion and absorption functions of the zebrafish. The results demonstrated that **DCQN** could be employed to visibly monitor the absorption and distribution of HSO_3^- in zebrafish during their growth and development period.

Experimental

Materials and characterizations

Unless specifically indicated, all reagents were supplied by Heowns-Reagent and Sigma-Aldrich, and used without further purification. ^{1}H and ^{13}C NMR spectra were acquired by using a Bruker AV spectrometer with tetramethylsilane (TMS) as an internal standard. High-resolution mass spectra (HRMS) were recorded by using an HP-1100 LC-MS spectrometer. UV-Vis absorption spectra were acquired by using a Hitachi UV-3310 spectrometer.

Fluorescence spectra were acquired by using a Hitachi FL-4500 fluorometer. Confocal fluorescence microscopy images of MCF-7 cells were acquired by using a Nikon A1 laser-scanning confocal microscope with a 100× objective lens (numerical aperture of the objective: 100×/1.4 oil (DIC N2), OFN, Plan Apo VC, Nikon Company; immersion oil, type: NF, nd = 1.515 (23 °C); microscope: Ti microscope, light path: L100, condenser: 3 (DIC N2)). Confocal fluorescence microscopy images of zebrafish were acquired by using a Nikon A1 laser-scanning confocal microscope with 4× objective lens (numerical aperture of the objective: 4×/0.2 dry (DIC N2), OFN, Plan Apo, Nikon Company).

Synthesis of DCIQ

DCI (300 mg, 1.61 mmol), which was prepared according to the literature,[48] along with 3-quinolinecarboxaldehyde (276 mg, 1.76 mmol), piperidine (25 μL, 0.25 mmol) and 25 mL anhydrous ethanol were refluxed for 7 h under an N_2 atmosphere. Then, the reaction mixture was cooled down, and the solvent was evaporated using a rotary evaporator. The residual mixture was purified by performing silica gel chromatography (eluent: CH_2Cl_2/ethanol = 60/1, v/v) to give the yellow solid DCIQ (323 mg, yield: 68%). ^{1}H NMR (400 MHz, DMSO-d_6) δ 9.25 (s, 1H), 8.65 (s, 1H), 8.04–8.02 (d, J = 8.0 Hz, 1H), 7.99–7.79 (d, J = 8.0 Hz, 1H), 7.81–7.77 (t, J = 8.0 Hz, 1H), 7.76–7.72 (d, J = 16.0 Hz, 1H), 7.67–7.63 (t, J = 8.0 Hz, 1H), 7.52–7.48 (d, J = 16.0 Hz, 1H), 6.98 (s, 1H), 2.66 (s, 2H), 2.61 (s, 2H), 1.05 (s, 6H). ^{13}C NMR (100 MHz, DMSO-d_6) δ 170.7, 155.7, 150.5, 147.9, 134.6, 131.9, 129.7, 129.6, 129.3, 129.0, 128.0, 127.8, 124.1, 114.2, 113.4, 77.7, 42.7, 38.5, 32.2, 27.9. HRMS(ESI): m/z: $[M + H]^+$ calcd for $C_{22}H_{20}N_3$: 326.1657; found: 326.1669.

Synthesis of DCQN

DCIQ (200 mg, 614.6 μmol), methyl trifluoromethanesulfonate (278 mL, 2.46 mmol) and 15 mL of dry dichloromethane were stirred for 12 h at ambient conditions. The reaction solution was concentrated to 1 mL by using a rotary evaporator, and then poured into a flask containing 10 mL of n-hexane to precipitate the yellow solid **DCQN** (412 mg, yield: 85%). ^{1}H NMR (400 MHz, DMSO-d_6) δ 9.90 (s, 1H), 9.40 (s, 1H), 8.52–8.50 (d, J = 8.0 Hz, 1H), 8.41–8.39 (d, J = 8.0 Hz, 1H), 8.30–8.25 (t, J = 10.0 Hz, 1H), 8.09–8.05 (t, J = 8.0 Hz, 1H), 7.80–7.76 (d, J = 16.0 Hz, 1H), 7.55-7.51 (d, J = 16.0 Hz, 1H), 6.97 (s, 1H), 4.64 (s, 3H), 2.70 (s, 2H), 2.60 (s, 2H), 1.07 (s, 6H). ^{13}C NMR (100 MHz, DMSO-d_6) δ 170.4, 154.1, 143.7, 137.9, 136.0, 134.9, 131.0, 130.7, 129.4, 125.6, 122.7, 119.8, 119.5, 113.8, 113.2, 79.5, 46.2, 38.5, 32.2, 27.9. HRMS (ESI): m/z: $[M]^+$ calcd for $C_{24}H_{22}F_3N_3O_3S$: 340.1808; found: 340.1811.

Cell cultures and fluorescence imaging

MCF-7 cells were cultured in Dulbecco's modified Eagle's medium (DMEM) supplemented with 10% fetal bovine serum (FBS, Invitrogen Corp., Carlsbad, CA) and penicillin–streptomycin (100 units per ml of penicillin and 100 μg per ml of streptomycin, Invitrogen Corp., Carlsbad, CA) at 37 °C in an incubator of air with 5% CO_2 and constant humidity. Before each imaging experiment was carried out, MCF-7 cells (2×10^4 cells per mL) were seeded in a 35 mm glass bottom dish (D110100, Matsunami, Japan) for 24 h. **DCQN** (10 μM) was added to the MCF-7 cells and incubated for 30 min at 37 °C. After that, the sample to be imaged was washed with PBS buffer (pH = 7.4) three times to remove the residual **DCQN**. Then to each sample of cells was added a different concentration of HSO_3^- (0, 30, 60 μM), and the resulting samples were incubated for 10 min, after which fluorescence images were acquired of them using a Nikon A1 confocal laser-scanning microscope.

Fluorescence imaging in zebrafish

Three-day post-fertilization zebrafish were purchased from Nanjing EzeRinka Biotechnology Co., Ltd. These zebrafish were cultured at 28 °C in the embryo medium supplemented with 1-phenyl-2-thiourea (PTU). To explore the performance of **DCQN** for imaging HSO_3^- in the 4-day old zebrafish, samples of these zebrafish were incubated with embryo medium containing **DCQN** (10 μM) for 30 min. Then, they were washed with embryo medium three times, and further incubated with HSO_3^- solution (0, 30, 60, 90, 120 μM) for 10 min. All zebrafish samples were washed three times with embryo medium before being imaged using a Nikon A1 confocal laser – scanning microscope. To determine HSO_3^- levels arising from the process of H_2O_2-induced oxidative stress, a control fluorescence imaging experiment involving H_2O_2 was also carried out. First, the zebrafish samples were incubated with **DCQN** (10 μM) for 30 min and then treated with HSO_3^- (120 μM) for 10 min. Then they were incubated with different concentrations (60, 90, 120, 240 μM) of H_2O_2 for 10 min at 28 °C. All zebrafish samples were washed three times with embryo medium and then images of them were acquired with a Nikon A1 confocal laser – scanning microscope.

Conclusions

In conclusion, a highly specific, rapidly responsive, mitochondrion-targeting near-infrared fluorescent probe, **DCQN**, was rationally prepared for the *in situ* monitoring of HSO_3^- *in vivo*. **DCQN** could be used to determine the concentration of HSO_3^- with high sensitivity (detection limit of 24 nM), a large Stokes shift (~110 nm) and a very rapid response (6 s). Moreover, **DCQN** was indicated to be quite biocompatible and was successfully used to image exogenous HSO_3^- in the mitochondria of live breast cancer (MCF-7) cells with large NIR fluorescence enhancement and a high contrast ratio. Moreover, **DCQN** was successfully used to image HSO_3^- in zebrafish with activated NIR emission during their growth and development processes (3–6 days). The excellent NIR emission, rapid response and *in situ*-activatable fluorescence features make **DCQN** an ideal imaging agent for visualizing sulfur dioxide derivatives in live organisms.

Conflicts of interest

All authors of this work declare no research conflicts.

Acknowledgements

This work was sponsored by the National Natural Science Foundation of China (No. 21978222, 31960720, 31560712), and the Natural Science Foundation of Tianjin (No. 17JCYBJC19600, 18JCYBJC94900). Ruilong Sheng appreciates support from Fundação para a Ciência e a Tecnologia (FCT project PEst-OE/QUI/UI0674/2019, CQM, Portuguese government funds), ARDITI-Agência Regional para o Desenvolvimento da Investigação Tecnologia e Inovação through the project M1420-01-0145-FEDER-000005-Centro de Química da Madeira-CQM+ (Madeira 14-20 Program) and ARDITI-2017-ISG-003.

Notes and references

1 K. K. Bertine and E. D. Goldberg, *Science*, 1971, **173**, 233–235.
2 W. Chen, Q. Fang, D. Yang and X. J. Foley, *Anal. Chem.*, 2015, **87**, 609–616.
3 A. Heagle, D. Body and W. W. Heck, *J. Environ. Qual.*, 1973, **2**, 365–368.
4 N. Sang, Y. Yun, H. Li, L. Hou, M. Han and G. Li, *Toxicol. Sci*, 2010, **114**(2), 226–236.
5 X. Shi, *J. Inorg. Biochem.*, 1994, **56**, 155–165.
6 T. Finkel and N. J. Holbrook, *Nature*, 2000, **408**, 239–247.
7 Y. Sun, J. Liu, J. Zhang, T. Yang and W. Guo, *Chem. Commun.*, 2013, **49**(26), 2637–2639.
8 J. Xu, J. Pan, X. Jiang, C. Qin, L. Zeng, H. Zhang and J. F. Zhang, *Biosens. Bioelectron.*, 2016, **77**, 725–732.
9 W. Zhang, T. Liu, F. Huo, P. Ning, X. Meng and C. Yin, *Anal. Chem.*, 2017, **89**(15), 8079–8083.
10 H. Jin, A. Liu, L. Holmberg, M. Zhao, S. Chen, J. Yang, Y. Sun, S. Chen, C. Tang and J. Du, *Int. J. Mol. Sci.*, 2013, **14**, 10465–10482.
11 G. Fang, X. Yang, W. Wang, Y. Feng, W. Zhang, Y. Huang, C. Sun, M. Chen and X. Meng, *Sens. Actuators, B*, 2019, **297**, 126777.
12 G. Chen, W. Zhou, C. Zhao, Y. Liu, T. Chen, Y. Li and B. Tang, *Anal. Chem.*, 2018, **90**, 12442–12448.
13 S. W. Tait and D. R. Green, *Nat. Rev. Mol. Cell Biol.*, 2010, **11**, 621–632.
14 K. Luby-Phelps, *Int. Rev. Cytol.*, 1999, **192**, 189–221.
15 W. Xu, C. L. Teoh, J. Peng, D. Su, L. Yuan and Y. T. Chang, *Biomaterials*, 2015, **56**, 1–9.
16 D. P. Li, Z. Y. Wang, X. J. Cao, J. Cui, X. Wang, H. Z. Cui, J. Y. Miao and B.-X. Zhao, *Chem. Commun.*, 2016, **52**, 2760–2763.
17 L. Yuan, W. Lin, J. Song and Y. Yang, *Chem. Commun.*, 2011, **47**, 12691–12693.
18 Y. Yang, L. He, K. Xu and W. Lin, *Anal. Methods*, 2019, **11**, 3931–3935.
19 Y. Yan, X. He, J. Miao and B.-X. Zhao, *J. Mater. Chem. B*, 2019, **7**, 6585–6591.
20 L. Yuan, W. Lin, Y. Xie, B. Chen and J. Song, *Chem. – Eur. J.*, 2012, **18**, 2700–2706.
21 D. Cheng, Y. Pan, L. Wang, Z. Zeng, L. Yuan, X. Zhang and Y. T. Chang, *J. Am. Chem. Soc.*, 2017, **139**, 285–292.
22 Z. Ye, C. Duan, R. Sheng, J. Xu, H. Wang and L. Zeng, *Talanta*, 2018, **176**, 389–396.
23 J. Xu, H. Yuan, L. Zeng and G. Bao, *Chin. Chem. Lett.*, 2018, **29**, 1456–1464.
24 M.-Y. Wu, K. Li, C.-Y. Li, J.-T. Hou and X.-Q. Yu, *Chem. Commun.*, 2014, **50**(2), 183–185.
25 J. Wu, J. Pan, Z. Ye, L. Zeng and D. Su, *Sens. Actuators, B*, 2018, **274**, 274–284.
26 Y. Zhao, Y. Ma and W. Lin, *Sens. Actuators, B*, 2018, **268**, 157–163.
27 C. Duan, M. Won, P. Verwilst, J. Xu, H. Kim, L. Zeng and J. Kim, *Anal. Chem.*, 2019, **96**, 4172–4178.
28 J.-T. Hou, H. Kim, C. Duan, M. Ji, S. Wang, L. Zeng, W. Ren and J. Kim, *Chem. Commun.*, 2019, **55**, 2533–2536.
29 X. Cheng, H. Jia, J. Feng, J. Qin and Z. Li, *Sens. Actuators, B*, 2013, **184**, 274–280.
30 C. Yin, X. Li, Y. Yue, J. Chao, Y. Zhang and F. Huo, *Sens. Actuators, B*, 2017, **246**, 615–622.
31 X. Ma, C. Liu, Q. Shan, G. Wei, D. Wei and Y. Du, *Sens. Actuators, B*, 2013, **188**, 1196–1200.
32 M. G. Choi, J. Hwang, S. Eor and S.-K. Chang, *Org. Lett.*, 2010, **12**, 5624–5627.
33 S. Chen, P. Hou, J. Wang and X. Song, *RSC Adv.*, 2012, **2**, 10869–10873.
34 Y. Liu, K. Li, K.-X. Xie, L.-L. Li, K.-K. Yu, X. Wang and X.-Q. Yu, *Chem. Commun.*, 2016, **52**(16), 3430–3433.
35 W.-L. Wu, H.-L. Ma, M.-F. Huang, J.-Y. Miao and B.-X. Zhao, *Sens. Actuators, B*, 2017, **241**, 239–244.
36 C. Duan, J. Zhang, Y. Hu, L. Zeng, D. Su and G.-M. Bao, *Dyes Pigm.*, 2019, **162**, 459–465.
37 Y. Sun, C. Zhong, R. Gong, H. Mu and E. Fu, *J. Org. Chem.*, 2009, **74**, 7943–7946.
38 L. Tang, P. He, X. Yan, J. Sun, K. Zhong, S. Hou and Y. Bian, *Sens. Actuators, B*, 2017, **247**, 421–427.
39 Q. Sun, W. Zhang and J. Qian, *Talanta*, 2017, **162**, 107–113.
40 Y. Liu, J. Nie, J. Niu, W. Wang and W. Lin, *J. Mater. Chem. B*, 2018, **6**(13), 1973–1983.
41 H. Agarwalla, S. Pal, A. Paul, Y. W. Jun, J. Bae, K. H. Ahn, D. N. Srivastava and A. Das, *J. Mater. Chem. B*, 2016, **4**, 7888–7894.
42 W. Zhang, F. Huo, Y. Zhang, J. Chao and C. Yin, *Sens. Actuators, B*, 2019, **297**, 126747.
43 L. Yuan, W. Lin, K. Zheng, L. He and W. Huang, *Chem. Soc. Rev.*, 2013, **42**, 622–661.
44 G. Yeap, E. Hrishikesan and Y. Chan, *J. Fluoresc.*, 2017, **27**, 105–110.
45 J.-H. Jeonga, J.-S. Kim, J. Campob, S.-H. Leea, W.-Y. Jeona, W. Wenseleersb, M. Jazbinsekc, H. Yund and O.-P. Kwona, *Dyes Pigm.*, 2015, **113**, 8–17.
46 Z. Meng, B. Zhang, J. Bai, H. Geng and C. Liu, *Inhalation Toxicol.*, 2003, **15**, 397–410.
47 Z. Meng, R. Li and X. Zhang, *Inhalation Toxicol.*, 2005, **17**, 309–313.
48 Z. Gao, X. Zhang, M. Zheng and Y. Chen, *Dyes Pigm.*, 2015, **120**, 37–43.